NANO LETTERS

pubs.acs.org/NanoLett

Reproducible, High-Throughput Synthesis of Colloidal Nanocrystals for Optimization in Multidimensional Parameter Space

Emory M. Chan,[†] Chenxu Xu,[†] Alvin W. Mao,[†] Gang Han,[†] Jonathan S. Owen,[‡] Bruce E. Cohen,[†] and Delia J. Milliron*[,†]

[†]The Molecular Foundry, Lawrence Berkeley National Laboratory, Berkeley, California 94720 and [‡]Department of Chemistry, University of California, Berkeley, California 94720

ABSTRACT While colloidal nanocrystals hold tremendous potential for both enhancing fundamental understanding of materials scaling and enabling advanced technologies, progress in both realms can be inhibited by the limited reproducibility of traditional synthetic methods and by the difficulty of optimizing syntheses over a large number of synthetic parameters. Here, we describe an automated platform for the reproducible synthesis of colloidal nanocrystals and for the high-throughput optimization of physical properties relevant to emerging applications of nanomaterials. This robotic platform enables precise control over reaction conditions while performing workflows analogous to those of traditional flask syntheses. We demonstrate control over the size, size distribution, kinetics, and concentration of reactions by synthesizing CdSe nanocrystals with 0.2% coefficient of variation in the mean diameters across an array of batch reactors and over multiple runs. Leveraging this precise control along with high-throughput optical and diffraction characterization, we effectively map multidimensional parameter space to tune the size and polydispersity of CdSe nanocrystals, to maximize the photoluminescence efficiency of CdTe nanocrystals, and to control the crystal phase and maximize the upconverted luminescence of lanthanide-doped $NaYF_4$ nanocrystals. On the basis of these demonstrative examples, we conclude that this automated synthesis approach will be of great utility for the development of diverse colloidal nanomaterials for electronic assemblies, luminescent biological labels, electroluminescent devices, and other emerging applications.

KEYWORDS Colloidal, synthesis, automation, optimization, high-throughput

Colloidal inorganic nanocrystals exhibit unique physical characteristics, such as size-dependent optical properties,[1,2] the ability to self-assemble into larger structures such as superlattices,[3] and crystal structures that differ in phase[4] or stability[5,6] with respect to bulk materials. Such properties have led to growing use of nanocrystals as luminescent biological labels,[7−9] in light-emitting diodes,[10,11] and in nanoscale electronic devices.[12−14] The investigation of nanocrystal properties and the development of their applications both rely on synthetic routes that are tunable and reproducible. In addition, synthetic optimization is required to meet the critical demands placed on material characteristics relevant to each application. For example, size distributions must be minimized in order to assemble ordered nanoparticle superlattices and to achieve efficient charge transport through these assemblies.[3,14,15] On the other hand, for application as biological labels or in light-emitting diodes, the photoluminescence quantum yield of nanocrystal quantum dots must be maximized. Finally, the magnetic, optical, and electrical properties of nanomaterials all depend strongly on their specific crystal phase, which therefore must be controlled synthetically.

Optimizing these nanomaterial properties and correlating them to reaction parameters, however, can be tedious and complex, due to the large number of synthetic variables that are critical for nanocrystal growth.[16,17] In addition to the selection of effective reagents and the optimization of their concentrations, the reaction temperature can be modulated over time to tune nucleation and growth, which often determine particle size,[18] shape,[19,20] and polydispersity.[21] While the manipulation of these parameters has created a rich diversity of colloidal nanomaterials,[21,22] the empirical rules discovered for the controlled synthesis of one chemical system do not necessarily transfer to others, so the development of each new material poses a fresh synthetic challenge.

The systematic exploration of parameter space for fundamental investigation and for the optimization of properties is further complicated by the limited reproducibility of many traditional synthetic methods. Solution-phase syntheses of single-crystalline and monodisperse colloidal nanomaterials often involve processes with sensitive kinetics[23,24] that can be altered by heating and cooling rates, side reactions,[25,26] and the presence of impurities.[20,27−29] Common methods also feature unpredictable transport phenomena, such as the rapid injection of reactive precursors into surfactant rapidly stirred at high temperature.[2,18] Such operations are difficult to control and to scale, particularly across users and labo-

* To whom correspondence should be addressed. Phone: 510-486-6723. Fax: 510-486-6166. E-mail: DMilliron@lbl.gov.
Received for review: 02/24/2010
Published on Web: 04/13/2010

DOI: 10.1021/nl100669s | *Nano Lett.* **2010,** *10,* 1874–1885

ratories, hindering the systematic development of nanomaterials chemistry.

In principle, automation may offer a means for precisely controlling reaction parameters, for facilitating multiplex screening, and for accelerating the optimization of physical properties.[30] Combinatorial approaches for the synthesis of inorganic nanomaterials, while not necessarily automated, have been used to synthesize nanomaterials heterogeneously on substrates via pulsed laser deposition,[31] chemical vapor deposition,[32] electrodeposition,[33] and biomolecular templating.[34,35] Automated, solution-phase syntheses of colloidal nanomaterials[36] to date have primarily adopted flow geometries such as stopped-flow,[37] continuous flow,[38−41] and segmented-flow reactors.[24,42] While such flow reactors have facilitated investigations into their reported growth reactions, these reactors are restricted to a narrow set of reagents and conditions due to issues such as reactor fouling, reagent compatibility, and broad residence time distributions.[24,43,44] This lack of flexibility limits the utility of these reactors for general nanomaterials research, optimization, and discovery. Thus, a flexible and general method for the automated synthesis of nanomaterials is still lacking.

Here, we describe an automated platform capable of synthesizing a diverse set of nanomaterials with exceptional reproducibility, and we present efficient methods for optimizing characteristics of these nanomaterials relevant to emerging applications. This automated platform can be applied to a wide range of materials because it uses reaction conditions and workflows that are directly analogous to those of traditional flask syntheses. Liquid handling robotics mimic traditional synthetic operations, such as sampling aliquots and injecting organometallic reagents into hot surfactant solutions. Unlike more restricted high-throughput methods, reaction solutions are contained in reagent-tolerant, disposable glass vials heated in an array of independently controlled reactors. And unlike manual experiments, products are characterized rapidly using high-throughput analytical tools. Leveraging these automated capabilities, we efficiently map multidimensional parameter space to investigate reaction pathways and to target optimization goals including tuning the size while minimizing the polydispersity of CdSe nanocrystals, maximizing the photoluminescence efficiency while minimizing the peak width of CdTe nanocrystals, and controlling the crystal phase to maximize the upconverted luminescence of rare earth-doped $NaYF_4$ nanocrystals.

Instrumentation. The foundation of our automated synthesis platform - the Workstation for Automated Nanomaterials Discovery and Analysis (WANDA) - is a Symyx Technologies Core Module deck (Figure 1a) with liquid-handing robotics for transferring solutions, a heated needle for dispensing molten surfactants, a vial-gripper for manipulating solid objects, and an automated balance for recording sample masses. Because the synthesis of high-quality nanomaterials often requires temperatures (~300 °C) that are much higher than those used for solution-phase reactions of small molecules, we developed a custom deck element with an array of eight high temperature reactors. As shown in Figure 1b, each of the eight Low Thermal Mass Reactor (LTMR) elements features independent temperature control and digitally tuned magnetic stirring to control the heat and mass transport of solutions contained in 40-mL glass vials, which serve as disposable reaction vessels that eliminate cross-contamination. Due to their low thermal mass, the reactors can be heated controllably to specified synthesis

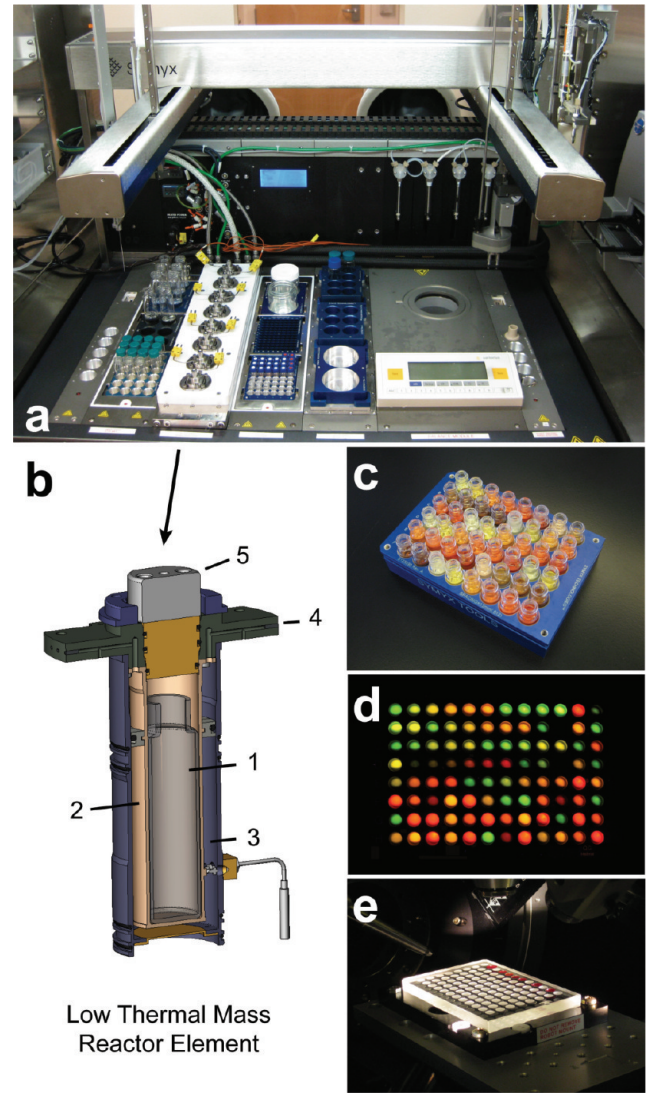

FIGURE 1. Workstation for Automated Nanomaterials Discovery and Analysis (WANDA). (a) Robotic deck featuring two liquid-dispensing robotic arms and an eight-element Low-Thermal Mass Reactor (LTMR) array for high-temperature nanocrystal synthesis. (b) Cross section of an LTMR element. A 40 mL glass vial (1) is inserted into the heated reactor cell (2), which can be cooled rapidly by nitrogen flow into the cooling shroud (3). Reactive gases can be injected through inlets (4), and the reactor can be accessed through configurable caps (5) that allow for pressurization or vacuum purging. (c) CdSe nanocrystal aliquots sampled by the robotic arms. (d) Photoluminescence of CdSe and CdTe nanocrystal aliquots in a 96-well quartz microplate. (e) Ninety-six-well glass X-ray diffraction plate for high-throughput X-ray diffraction.

DOI: 10.1021/nl100669s | *Nano Lett.* **2010,** *10,* 1874–1885

temperatures up to 350 °C at specified rates up to 40 °C/min. The reactors can be cooled at rates exceeding 60 °C/min using nitrogen flow forced through a shroud surrounding each reactor. Solutions can be accessed through ports in the removable reactor caps, which allow for vacuum purging or for the pressurized injection of reaction gases via inlets that interface with the caps.

For high-throughput characterization of products and aliquots (Figure 1c), absorption and photoluminescence spectra are acquired in a 96-well quartz microtiter plate (Figure 1d) using a Biotek Synergy4 multifunction microplate reader. The plate reader is also used to measure upconversion luminescence intensities of solid nanocrystal pellets using an 850 nm long pass excitation filter and a 550/100 nm bandpass emission filter. X-ray diffraction patterns are acquired on a glass XRD microwell plate (Figure 1e) using an external Bruker D8 Discover powder diffractometer equipped with an automated stage and a 2D (GADDS) detector to enhance throughput. Excluding the diffractometer, the entire apparatus is enclosed by a nitrogen-filled glovebox such that reagent preparation, reaction automation, product purification, and optical analysis are performed without exposing nanomaterials and reagents to oxygen or water.

Reproducible CdSe Nanocrystal Synthesis from Cadmium Oleate. To evaluate the ability of our automated platform to control reaction conditions and produce monodisperse nanocrystals for applications such as nanoscale assemblies, we performed replicate syntheses of CdSe nanocrystals across WANDA's reactor array and over multiple runs. Any variations in reaction parameters would perturb CdSe nanocrystal size and size distribution, which can be determined readily from optical spectra.[45] The high-temperature synthesis of CdSe nanocrystals from cadmium oleate (Cd-OLA), tri-*n*-octylphosphine selenide (TOPSe), and oleylamine (OM) in noncoordinating solvent can produce monodisperse nanocrystals with high-photoluminescence quantum yield.[40] Because of the instability of cadmium oleate precursors at high temperature in the presence of amines,[46,47] however, a delicate balance of reaction conditions must be maintained for the synthesis of nanocrystals with uniform properties.

The reproducibility of the absorption spectra (Figure 2a) from eight replicate CdSe reactions at six different reaction times demonstrates the precise control over reaction parameters conferred by automation. The absorption spectra are normalized only by aliquot weight, to quantitatively correct for any variations in aliquot volume. At each aliquot time (τ_{rxn}), the spectra from the eight LTMR reactors are nearly identical in the peak positions of their first exciton ($1S_{1/2}(e)-1S_{3/2}(h)$) transitions, their peak widths, spectral shapes, and overall intensities, indicating nanocrystals with reproducible size, size distribution, morphology, and concentration. Figure 2b shows the time dependence of the diameter, reaction yield, particle concentration, and the half

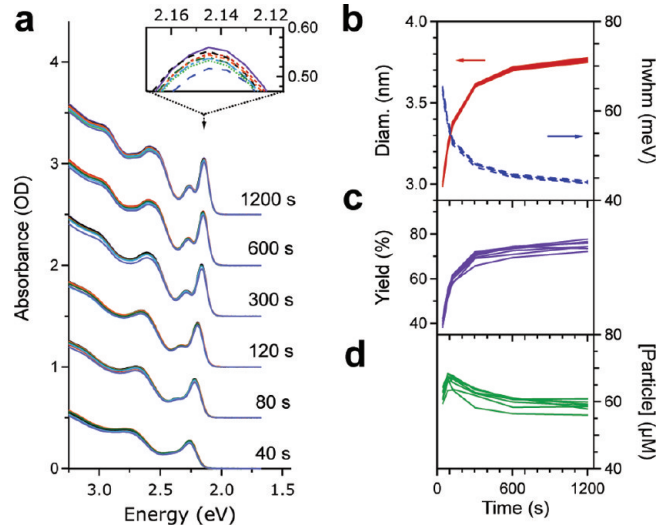

FIGURE 2. CdSe nanocrystal synthesis reproducibility across eight reactors. (a) Absorption spectra, normalized by aliquot mass, for 48 aliquots sampled from eight reactors at six aliquot times. Inset: Magnification of the $1S_{1/2}(e)-1S_{3/2}(h)$ peak region of the 1200 s spectra. Time dependent traces for (b) the diameter and the half width at half-maximum (hwhm) of the absorption peak, (c) yield, and (d) nanocrystal concentration for eight reactors. Reactions are performed at 260 °C with 40 mM cadmium oleate, 3:1 oleic acid/cadmium, 2:1 Se/Cd, and 0.5 M oleylamine.

width at half-maximum (hwhm) of the absorption peak, which varies with the size distribution. These time traces illustrate that the kinetics are extremely reproducible across the LTMR reactors, particularly in terms of size and size distribution.

The exquisite reproducibility of these automated reactions is further evinced by the narrow standard deviations (σ) of the CdSe nanocrystal parameters, as calculated across the 1200 s values for each reactor (Table 1, Robot Run 1). The coefficient of variation of the diameter values across the eight reactors is 0.2 % (CV = σ/μ, where μ is the mean). This variation lies well below the >1 % uncertainty in the spectroscopic sizing curve and peak-fitting algorithm, meaning that the diameters are statistically identical across the reactors. The size distributions of the nanocrystal populations inside each reactor also vary little from reactor to reactor with 0.5 % CV across the eight reactions. The reaction yield and nanocrystal concentration have somewhat larger variations across reactors (~3 % CV), which we ascribe to the intrinsic errors associated with liquid dispensing, solvent evaporation, and size estimation.

A relative size distribution of 9.12 %, averaged across the reactions in Robot Run 1 of Table 1, is spectroscopically determined from aliquot hwhm values. To assess the reliability of size dispersions derived from hwhm values, we also measured the physical size distribution using automated sizing methods on transmission electron micrographs (TEM). We observe a 9.5 % size distribution by TEM, (Figure S1, Supporting Information) in good agreement with the spectroscopic estimate, suggesting that hwhm values offer simple

DOI: 10.1021/nl100669s | *Nano Lett.* **2010,** *10,* 1874–1885

TABLE 1. Reproducibility of Automated and Manual CdSe Nanocrystal Syntheses[a]

run	*N*	diameter (nm)	relative size distribution (%)	hwhm (meV)	yield (%)	[particle] (μM)
robot no. 1	8	3.762 (9)[b]	9.12 (5)	44.0 (2)	75 (2)	59 (2)
robot no. 2	8	3.768 (9)	9.17 (5)	44.2 (2)	73 (2)	57 (2)
flask	6	3.67 (9)	12 (2)	57 (7)	85 (8)	72 (6)

[a] $T = 260$ °C, $\tau_{rxn} = 1200$ s with 40 mM cadmium oleate, 3:1 oleic acid/cadmium, 2:1 Se/Cd, and 0.5 M oleylamine. [b] Errors in parentheses correspond to one standard deviation across the *N* reactions in each run and are given in units of the last digit.

and accurate measures of polydispersities. Although the size distributions of these raw reaction solutions are broader than polydispersities reported elsewhere, our spectral widths (hwhm values) are as narrow as the best literature values. This apparent discrepancy can be explained by our use of automated sizing, which avoids unintentional bias in evaluating size distributions on the basis of TEM images. Thus, we have high confidence that WANDA can synthesize nanocrystals with narrow size distributions that are comparable to the best methods but with significantly higher precision.

To demonstrate the reproducibility of WANDA across multiple runs, we performed a second eight-reactor run of CdSe nanocrystal syntheses using the same reagents and conditions as the previous eight-reactor experiment. A comparison of the nanocrystal parameters from the two runs is given in Table 1. The mean values of the diameters, relative size distributions, hwhm, reaction yields, and particle concentrations for the 1200 s aliquots of the two CdSe runs all fall within one standard deviation, as calculated across the eight values for each run. This run-to-run reproducibility is especially notable given the minimal variation in the values across each run. Thus, from run to run, WANDA can synthesize nanocrystals with nearly identical size, size distribution, yield, and concentration.

To determine the quantitative advantage of WANDA over traditional methods, we performed a series of six manual CdSe nanocrystal syntheses using the same conditions and the same batches of reagents as those used for the automated CdSe reactions. By every metric, the automated syntheses are dramatically more reproducible than the manual syntheses (Table 1 and Supporting Information Figure S2). After 1200 s of growth, the manually synthesized nanocrystals exhibited diameters with 2.5% CV, an order of magnitude less precise than the 0.2% CV of either robot series. Similarly, the manual reaction yield and particle concentrations have variations three to four times larger than their robotic counterparts.

The most significant differences between the manual and automated syntheses were the size distributions of the nanocrystals derived from the hwhm values. Flask-synthesized nanocrystals exhibited an absorption hwhm of 57 meV $\pm$ 12% CV, compared to 44 meV $\pm$ 0.5% CV for nanoparticles synthesized in WANDA. These hwhm values correspond to size dispersions of 12 $\pm$ 2 and 9.12 $\pm$ 0.05% (absolute standard deviation) for the manual and automated syntheses, respectively. These size distributions demonstrate that the control and reproducibility of automation can significantly narrow the size distribution of nanocrystals and can maintain such distributions with a precision approximately 40 times greater than that of manual methods.

The manual syntheses also resulted in smaller particles at higher concentrations and with higher yield. When performing rapid TOPSe injections by hand, poor control over the dispensed volume and injection rate likely results in variations in nucleation kinetics, which ultimately determine particle size and concentration.

We note that the cadmium oleate/oleylamine/octadecene reaction solution, although clear at room temperature, turns cloudy brown at 260 °C, indicating the decomposition of Cd-OLA into CdO,[47] as verified by X-ray diffraction (XRD, Supporting Information Figure S3). Our results therefore contradict conventional wisdom that inhomogeneous precursor solutions produce poor size distributions and irreproducible results. We hypothesize that these insoluble species narrow size distribution by serving as a cadmium reservoir that does not participate readily in nucleation. After the TOPSe injection, the solutions become clear, indicating that solid cadmium species have redissolved so that this fraction of the cadmium is available for the growth, but not nucleation, of the nanocrystals. By moderating the cadmium precursor supersaturation over the course of the reaction, this precipitation process may be critical for focusing particle size distributions and delaying Ostwald ripening.[48] The formation of these insoluble species may be dependent on temperature ramp times and rates, which explains why manual syntheses result in broader size distributions with larger batch-to-batch variation while no such problems arise with WANDA given its highly reproducible reaction conditions.

Thus, the narrow and consistent size distributions observed with the automated CdSe syntheses are a direct result of WANDA's precise control over critical parameters such as reaction temperature and ramp rate, TOPSe injection rate and volume, and mixing rate and reaction time. Over the course of nine months, we have run the same CdSe reaction 40 times, using reagents of different purities from different vendors and batches. These chemical variations are apparently not significant for kinetics in this reaction system, since the variation in the diameters and size distributions of the nanocrystals from these 40 reactions was $\leq$1%, despite the differences in precursors. Such precise control is valuable for the synthesis of a wide range of nanomaterials, because size, size distribution, reaction yield, and concentration are critical parameters for any colloid reaction.

DOI: 10.1021/nl100669s | *Nano Lett.* **2010,** *10,* 1874–1885

Multidimensional Optimization of CdSe Nanocrystals Synthesized with Cadmium Oleate. The automated synthesis of CdSe nanocrystals from Cd-OLA offers a method to produce quantum dots with high chemical yield and low size distribution, yet most applications require broad size tunability as well. Because of the narrow range of sizes accessible to syntheses that utilize Cd-OLA, significant alterations in growth parameters are required to obtain particles with larger diameters (>5 nm).[47] Using the ability to systematically define reaction parameters over multiple reactors and multiple runs, we rapidly characterized broad areas of parameter space to synthesize monodisperse CdSe nanocrystals with a range of diameters and to characterize the chemical nature of any size limitations.

When mapping parameter space to identify the reaction conditions that produce the narrowest size distributions for each accessible diameter, we vary reaction time in addition to reagent concentrations and temperatures, because nanocrystal size distributions can narrow and broaden over the course of a reaction.[48] By densely mapping these reaction parameters and finding the conditions with the minimum hwhm at each spectroscopically determined diameter, we can rapidly isolate the conditions that produce the narrowest size distribution possible for each average nanocrystal size.

We use the hwhm to optimize CdSe nanocrystal reactions because it is a direct observable that can be determined with high precision. Although an approximate value for the physical size distribution can be derived from the hwhm (see Section IIB in the Supporting Information), this introduces additional error, compromising its utility as a figure of merit for synthetic optimization. Direct consideration of hwhm values is more precise and, additionally, since hwhm values are commonly reported, this facilitates comparison with the literature.

For the synthesis of CdSe nanocrystals, we demonstrated the concurrent tuning of size and the minimization of spectral peak width by independently varying the temperature, oleylamine concentration, cadmium oleate concentration, and TOPSe/Cd-OLA mole ratio, as shown in Figure 3 and Figure S4 (Supporting Information). Each two-dimensional optimization in Figure 3 shows the hwhm versus the diameter for each timed aliquot from 40 to 1200 s with a low hwhm (size distribution) across the entire size range being optimal.

The optimal temperature shown is 260 °C with the narrowest hwhm of 44 meV at $d = 3.8$ nm (Figure 3a). Increasing the reaction time beyond 1200 s increases the diameter little, and increasing the temperature accelerates the kinetics without affecting the dispersion at each size. In this reaction system, the size and size distribution alike are extremely sensitive to the oleylamine concentration. So, while changes in [OM] can be used to tune the size, increasing or decreasing [OM] from its optimal value of 0.5 M substantially broadens the size distribution (Figure 3b). Hence, rather than adjusting [OM], size can be more effectively tuned by changing the cadmium oleate concentration and the Se/Cd mole ratio, since decreasing either [Cd-OLA] or Se/Cd varies the nanocrystal diameter over a wider range with a less severe penalty on the hwhm at larger diameters (Figure 3c,d).

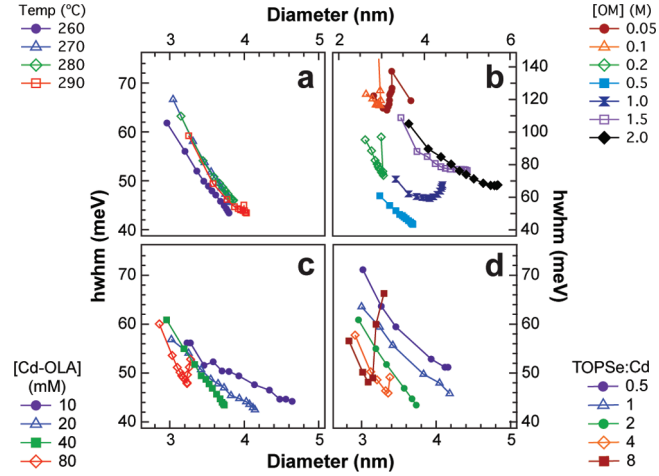

FIGURE 3. Optimization of CdSe nanocrystal growth parameters. Absorption hwhm vs diameter with varying temperature (a), oleylamine (OM) concentration (b), preinjection cadmium oleate (Cd-OLA) concentration (c), and TOPSe/Cd mole ratio (d). Linked markers denote aliquots from the same reaction taken at 40, 80, 120, 160, 200, 240, 300, 420, 600, 780, 960, and 1200 s (a−c) or 40, 80, 120, 300, 600, and 1200 s (d). Excluding the varied parameter for a given panel, the following conditions are maintained: 260 °C growth, 40 mM Cd-OLA, 3:1 oleic acid/cadmium, 2:1 TOPSe/Cd, and 0.5 M oleylamine.

To determine the optimal combination of [Cd-OLA], [TOPSe], and reaction time for each nanocrystal size, we performed a three-factor optimization by synthesizing CdSe nanocrystals at four Cd-OLA concentrations, five TOPSe concentrations, and six reaction times. Figure 4 shows the dependence of the diameter and hwhm on the [Cd-OLA], [TOPSe], and reaction time. The 2D projections on the faces of the 3D plot show the minimum hwhm and the diameter at the minimum hwhm (d_{min}) for each pair of TOPSe and Cd-OLA concentrations. It is apparent that decreasing [TOPSe] from 320 mM to 20 mM increases d_{min} monotonically from 3 to 5 nm. At high [TOPSe], the hwhm versus diameter traces become U-shaped due to rapid depletion of cadmium precursors, and optimum reaction times become shorter. While the diameter is strongly correlated to the TOPSe concentration, d_{min} is surprisingly invariant over 8-fold increases in the Cd-OLA concentration (Figure 4, bottom projection). Diameters only vary with [Cd-OLA] at long reaction times for reactions in which the TOPSe is depleted before the Cd-OLA.

The insensitivity of the diameter to drastic changes in [Cd-OLA] can be explained by analyzing the nucleation and growth of CdSe nanocrystals from this combination of reactants. Because WANDA enables the quantitative determination of the final (1200 s) nanoparticle concentrations from the reaction yields and diameters, it is readily apparent

DOI: 10.1021/nl100669s | *Nano Lett.* **2010,** *10,* 1874–1885

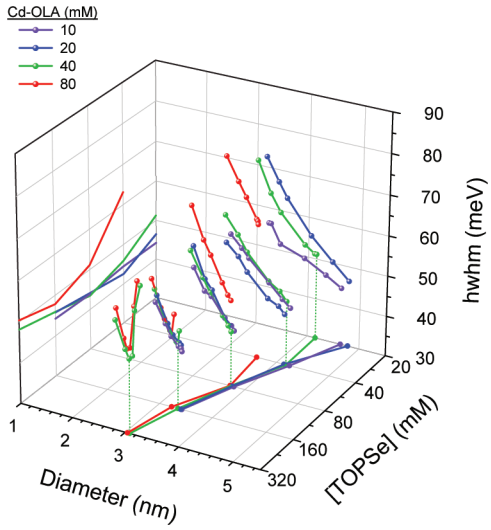

FIGURE 4. Absorption hwhm and diameter vs TOPSe concentration, Cd-OLA concentration, and reaction time. Linked markers in three-dimensional space denote aliquots taken at 40, 80, 120, 300, 600, and 1200 s. Projections on the left and bottom faces display the hwhm and diameter, respectively, at the time point with the minimum hwhm for each trace.

that increasing [Cd-OLA] and increasing [TOPSe] each result in higher concentrations of particles (Figure 5a). This final concentration is approximately the same as the particle concentration of nuclei during the growth phase, since the particle concentrations are not observed to change significantly over time (e.g., Figure 2d). The observed particle concentrations in Figure 5a exhibit a two-dimensional power law dependence in which

$$[\text{Particle}] = k_{\text{nuc}}[\text{Cd-OLA}]_0^{\,a}[\text{TOPSe}]_0^{\,b} \qquad (1)$$

and

$$\log[\text{Particle}] = \log k_{\text{nuc}} + a\log[\text{Cd-OLA}]_0 + b\log[\text{TOPSe}]_0 \qquad (2)$$

where $[\text{Cd-OLA}]_0$ and $[\text{TOPSe}]_0$ are the precursor concentrations immediately after the TOPSe injection. The fit parameters are $a = 0.94 \pm 0.04$ and $b = 0.58 \pm 0.03$ with an R^2 of 0.9895.

No cross terms ($[\text{Cd-OLA}]_0 \times [\text{TOPSe}]_0$) are needed to achieve a reasonable fit, implying that the effects of the two precursor concentrations on particle concentration are independent. The form of the eq 1, along with our findings that $a \sim 1$ and $b \sim 0.5$, indicates a possible link between nucleation and precursor reaction kinetics, which has been discussed by others[49] and the mechanistic implications of which we will explore further in a forthcoming publication. This empirical nucleation model, however, is already sufficient for analyzing nanocrystal growth in context with the available precursor per particle.

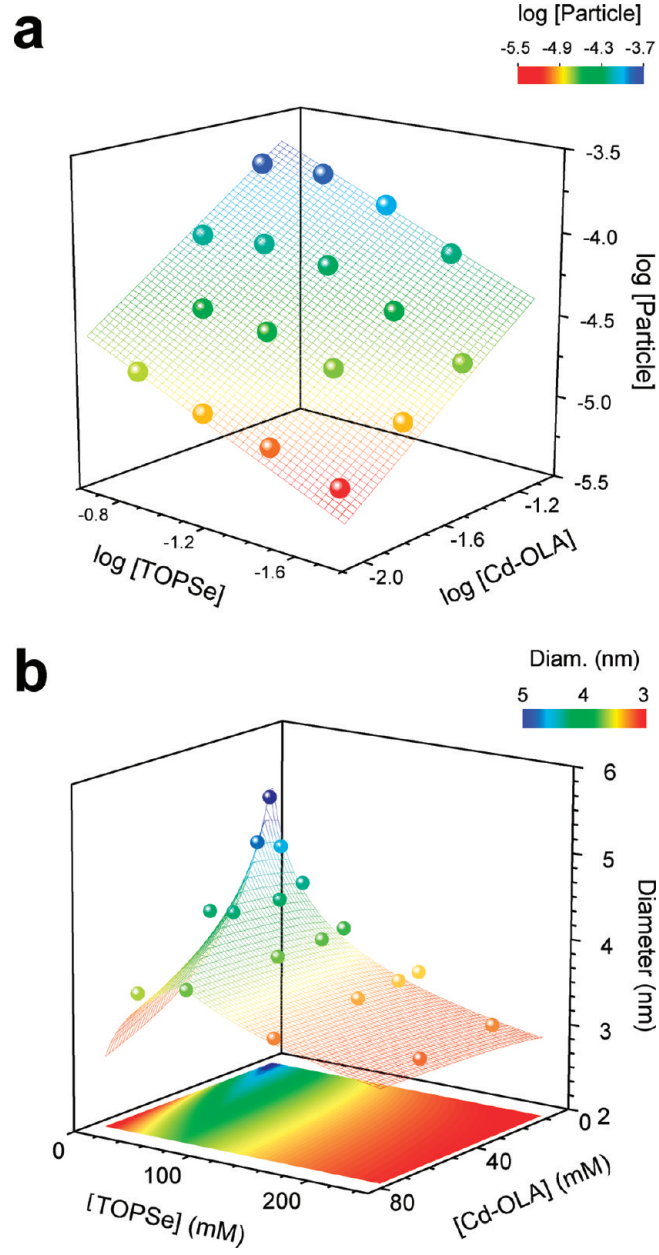

FIGURE 5. (a) Particle concentration vs post-injection cadmium oleate and TOPSe concentration in Molar for the CdSe nanocrystal reactions in Figure 4.The mesh plane fits the data points with the equation, $\log[\text{Particle}] = \log k_{\text{nuc}} + a\log[\text{Cd-OLA}] + b\log[\text{TOPSe}]$, where $\log k_{\text{nuc}} = -2.27(6)$, $a = 0.94$ (4), and $b = 0.58(3)$, with $R^2 = 0.990$. Reactions are conducted at 260 °C, 3:1 OLA/Cd, and 0.5 M oleylamine. (b) CdSe nanocrystal diameters observed at 1200 s vs diameters derived from the particle concentration model in (a), with $R^2 = 0.929$. The bottom face shows the projection of the modeled diameter.

The ability to estimate particle concentrations with eq 1 enables the straightforward prediction of the final nanocrystal diameters from the initial Cd-OLA and TOPSe concentrations, making the approximation that the fractional reaction yield is independent of these parameters. This simplification

DOI: 10.1021/nl100669s | *Nano Lett.* **2010,** *10,* 1874–1885

is supported by the data since, for a 1200 s reaction time, the fractional yield averaged across the reactions shown in Figure 4 is 0.72 ± 0.08. The moderate 12% standard deviation of this yield does not significantly reduce the precision of our diameter predictions, because the diameter of a sphere is proportional to the cube root of its volume, meaning that a relative uncertainty of 12% in the yield results in only a 4% uncertainty in the predicted diameter.

Using the mean reaction yield (Y_f), initial precursor concentrations, and the particle concentration from eq 1, one can calculate the number of CdSe molecular units per particle

$$N_{\mathrm{CdSe/Particle}} = Y_f[\mathrm{LR}]_0/[\mathrm{Particle}] \quad (3)$$

where $[LR]_0$ is the concentration of the limiting reagent, Cd-OLA or TOPSe, immediately following the TOPSe injection. Assuming a spherical nanocrystal with the molar volume, V_m, of bulk CdSe, the mean predicted diameter is

$$d_{\mathrm{predicted}} = \left(\frac{6V_m}{\pi}\frac{N_{\mathrm{CdSe/Particle}}}{N_A}\right)^{1/3} \quad (4)$$

where N_A is Avogadro's number.

The theoretical diameters (Figure 5b), calculated with eq 4 at 17 different combinations of [Cd-OLA] and [TOPSe], agree closely with observed diameters for the CdSe nanocrystals depicted in Figures 4 and 5a; the root-mean-squared (rms) difference between the theoretical and observed diameters is only 0.15 nm. At a diameter of 4 nm, this rms error is comparable to the 4% uncertainty propagated from the assumed reaction yield. The modeled data accurately describe the observed trend in which a combination of low [Cd-OLA] and [TOPSe] induces larger diameters. The ridge in the response surface in Figure 5b corresponds to [Cd-OLA] = [TOPSe], the transition point for the limiting reagent. At Se/Cd > 1, the model further predicts that the diameter is largely insensitive to [Cd-OLA], as we also observed in the experimental results (Figure 4). We can analytically explain this trend by the fact that the $[LR]_0$ term in eq 3 is canceled out by the $[\mathrm{Cd\text{-}OLA}]^a$ term in eq 1, since Cd-OLA is the limiting reagent, and since $a \sim 1$. Essentially, the final number of CdSe molecular units per particle remains constant despite changes in cadmium precursor concentration, because any increase in [Cd-OLA] induces a proportional increase in the number of nuclei.

Thus, in only three experiments using WANDA, employing eight reactors each, we have characterized reaction parameter space sufficiently to predict from initial reactant concentrations the nucleation behavior and the diameters of future CdSe nanocrystal syntheses. The 0.15 nm uncertainty in the diameters predicted by our empirical model is less than the thickness of one atomic monolayer, excellent precision considering our simplifying assumptions. While this empirical response function neglects the complex differential equations that govern the nucleation kinetics, size-dependent surface reactions, and transport phenomena that occur simultaneously in nanocrystal syntheses, there is tremendous utility in the ability to predict nanocrystal size and concentration without computationally intensive simulations.

Multidimensional Optimization of CdSe Nanocrystals Synthesized from Cadmium Octadecylphosphonate. Nanomaterials such as CdSe quantum dots can be synthesized using a variety of reagents with the optimal reaction conditions depending significantly on precursor reactivity and surfactant functionality. In cadmium chalcogenide nanocrystal flask reactions, trioctylphosphine oxide (TOPO) and cadmium alkylphosphonate complexes such as cadmium octadecylphosphonate (Cd-ODPA) are commonly used to synthesize high quality nanocrystals over wider ranges of sizes and shapes than are accessible with Cd-OLA and ODE.[16,21,22,50,51] Despite the popularity of Cd-ODPA and TOPO, the frequent discovery of impurities that influence the behavior of these reactions[20,27−29] emphasizes that the actual parameters for obtaining nanocrystals with targeted properties may be quite different than believed on the basis of initial reports, making reproduction of previous results uncertain and challenging. The use of purified surfactant along with high-throughput methods offers an accurate method to isolate ideal conditions that can be indefinitely reproduced and to perform the detailed multidimensional studies that probe mechanisms for such reactions.

For flow reactors, however, Cd-ODPA and TOPO are difficult to use because the chemicals are solid at ambient temperatures and because Cd-ODPA complexes can have poor solubility below 120 °C. Thus, to explore WANDA's compatibility with these reagents and to map the synthetic parameter space of such reactions, we performed a 3 × 4 × 16 factorial optimization of the ODPA/Cd mole ratio, Se/Cd mole ratio, and reaction time for the synthesis of CdSe nanocrystals with Cd-ODPA, TOPSe, and TOPO. Figure 6 shows the hwhm versus diameter for CdSe nanocrystals synthesized under these 192 conditions. For each diameter in each ODPA/Cd set, Figure 6 displays the results only from the Se/Cd set with the minimum hwhm out of the four Se/Cd mole ratios. Thus, for each surfactant concentration, only the "optimal" reaction conditions, the Se/Cd mole ratio and reaction time that produces the narrowest size distribution for each diameter, are shown.

We demonstrate the interpretation of these results for the case of ODPA/Cd = 1.72. For nanocrystals with diameter $d = 2.2-4.0$ nm, the narrowest hwhm values are achieved with Se/Cd = 2.0. The requisite reaction times range from 80 s for 2.2 nm particles to 360 s for 4.0 nm particles. For the synthesis of larger particles, however, the optimal conditions shift to substantially

DOI: 10.1021/nl100669s | Nano Lett. 2010, 10, 1874–1885

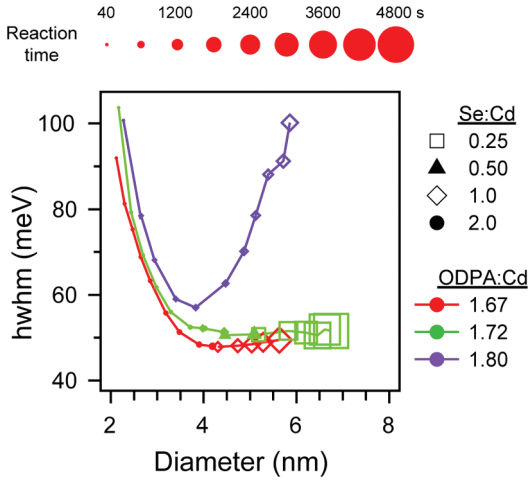

FIGURE 6. Optimization of CdSe nanocrystals synthesized from cadmium octadecylphosphonate (CdODPA). Absorption hwhm vs diameter at three ODPA/Cd mole ratios and four Se/Cd mole ratios. At each wavelength and ODPA/Cd ratio (colors), only the data points for the Se/Cd ratio (markers) with the minimum hwhm are displayed. Marker sizes scale linearly with reaction time.

lower Se/Cd and longer reaction times. The largest particles, with $d = 5.2-6.7$ nm, are achieved optimally with Se/Cd = 0.25 and reaction times of 1800 to 4800 s. Qualitatively, the low TOPSe concentration limits nucleation so that fewer particles are formed which then grow to larger final diameters, but the lower concentration also slows the reaction kinetics, requiring longer reaction times to achieve those large diameters.

The polydispersity of the CdSe nanocrystals in Figure 6 is decreased by reducing ODPA/Cd with small decreases in ODPA/Cd resulting in significant decreases in the hwhm at all diameters. This result is particularly notable since the tedium of varying synthetic parameters has generally discouraged previous researchers from testing conditions below the stoichiometric ratio of two alkylphosphonic acid equivalents per cadmium for the formation of cadmium dialkylphosphonate precursor. The disadvantage of low ODPA/Cd ratios is that the maximum particle sizes are limited; at ODPA/Cd = 1.67, the largest diameter observed is 5.6 nm. Increasing the reaction time beyond 2400 s results in bimodal size distributions, while decreasing Se/Cd < 1.0 increases the hwhm without achieving larger diameters. Thus, the optimal ODPA/Cd for particles larger than 5.6 nm is ODPA/Cd = 1.72. Further increases in the ODPA/Cd, as shown with ODPA/Cd = 1.8, however result in more polydisperse particle populations.

Compared to this synthesis with Cd-ODPA, CdSe syntheses with Cd-OLA generally produce CdSe nanocrystals with narrower size distributions with hwhm ~44 meV. The slower kinetics and lower reactivity of Cd-ODPA, however, enable the synthesis of a wider range of nanocrystal sizes and shapes. The flexibility to use both sets of reagents in WANDA enables users to optimize nanomaterials with a diverse set of physical properties regardless of reaction requirements.

Optimization of CdTe Nanocrystal Photoluminescence. Several emerging applications of nanocrystal quantum dots rely on highly efficient, size-tunable luminescence. For biological imaging,[9] small diameters are critical for minimizing physical interference with biological processes, and narrow, green to near-infrared emission with high quantum yield is desirable for maximizing signal from probes in cells or tissue. This combination of requirements makes CdTe nanocrystals an appealing material choice. We synthesized CdTe nanocrystals from CdO, oleic acid, and octadecene,[52,53] and as for the case of CdSe, the equilibrium between CdO and cadmium oleate plays a critical role in the growth of monodisperse particles. In addition, few reports have explored OLA/Cd ratios that are too low to drive the full conversion of CdO to Cd-OLA. Since CdTe reaction kinetics are sensitive to the chemical behavior of ligands coordinated to nanocrystal surfaces and to precursors, we examined the effect of the oleic acid concentration on CdTe size and photoluminescence (PL).

Using WANDA, we synthesized a series of CdTe nanocrystals in which we varied the oleic acid/CdO mole ratio (OLA/Cd) from 1.3 to 4.7. Figure 7a shows the effect of OLA/Cd on the diameter, the full-width-at-half-maximum (fwhm) of the PL peak, and the normalized PL intensity. The PL intensity is integrated from 1.55 to 2.45 eV and is then normalized by the absorbance at the excitation wavelength of 380 nm in order to quickly estimate the relative PL efficiency between samples. The CdTe nanocrystals exhibit a maximum PL efficiency at OLA/Cd of 2.7 with 3.68 nm diameter and 200 s growth time (Figure 7a). As shown in Figure 7b, the 121 meV nm fwhm of these 3.7 nm particles is not the minimum possible fwhm for this size (101 meV), which demonstrates that achieving optimal conditions for a given application may involve compromising other properties. Further optimization of orthogonal reaction parameters could potentially reduce this size distribution while maintaining high PL efficiency. Alternatively, the nanocrystal properties can be weighted by preference to enable the calculation of a single satisfaction coefficient, which can maximized using the detailed information in Figure 7.[17]

The relationship between the diameter and OLA/Cd mole ratio is also nonmonotonic (Figure 7a), exhibiting a minimum at 2.7 OLA/Cd that coincides with the maximum in PL efficiency. Shifting the OLA/Cd above or below 2.7 results in larger diameter particles, suggesting two regimes in CdTe growth. Below 2.7:1 OLA/Cd, the conversion of CdO to cadmium oleate is incomplete, leading to insoluble reservoirs of CdO. Although Kloper et al.[53] observed Cd metal nanoparticles precipitating from Cd-OLA/ODE solutions, precipitates in this CdTe experiment have a distinctive dark brown appearance under nitrogen and are verified to be CdO by XRD (Supporting Information Figure S5). The insoluble CdO at OLA/Cd less than 2.7:1 reduces the cadmium oleate

DOI: 10.1021/nl100669s | *Nano Lett.* **2010,** *10,* 1874–1885

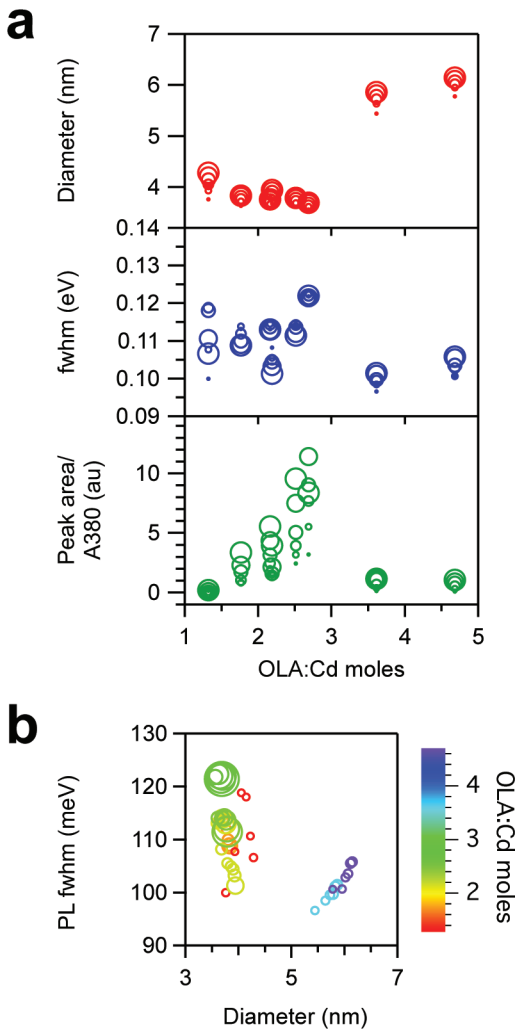

FIGURE 7. (a) Dependence of CdTe diameter, photoluminescence (PL) full width at half-maximum (fwhm), and integrated PL intensity normalized by the absorbance at 380 nm, on the oleic acid−cadmium oxide (OLA/Cd) mole ratio. Marker size increases with reaction time (40−240 s in 40 s increments). (b) PL fwhm vs diameter. Colors represent OLA/Cd, while markers increase in size with normalized fluorescence intensity. CdTe nanocrystals are grown at 300/265 °C injection/growth temperature with 17 mM CdO and 1:1.2 Te/Cd mole ratio.

available for nucleation, and, as that CdO dissolves during particle growth, subsequently increases the cadmium available for growth on fewer nuclei. Above 2.7:1 OLA/Cd, the CdO is completely converted to cadmium oleate before injection, and the excess oleic acid suppresses nucleation,[54,55] leading to larger particles. The rapid identification of such distinct reaction regimes and their implications on critical characteristics such as PL efficiency is facilitated by a precise, multiplexed platform.

Optimization of Crystal Structure and Upconversion Luminescence in Rare Earth-Doped $NaYF_4$ Nanocrystals. In addition to size, polydispersity, and photoluminescence, the crystallinity of nanocrystals is often a vital characteristic, and we sought to determine whether WANDA could optimize synthetic control over the crystal structures of colloidal nanomaterials. $NaYF_4$ nanocrystals doped with Yb^{3+} and Er^{3+} exhibit strong upconverted luminescence[56] in the visible region when excited with 980 nm continuous wave laser excitation, but the quantum efficiency of this anti-Stokes emission is strongly dependent on the phonon energies and thus the crystal phase of the host $NaYF_4$ matrix.[57] The hexagonal, gagarinite-like β-$NaYF_4$ phase, with its 9-fold coordinated rare earth ions and its low phonon energies,[57] gives rise to over four times more efficient upconversion than the cubic, fluorite-like α-$NaYF_4$.[58] Recent synthetic methods for doped $NaYF_4$ nanocrystals can produce both α- and β-$NaYF_4$, and transitions between existing phases can be modulated by surfactants such as oleic acid.[59−61] Mapping the stability of the two crystal phases in the presence of oleic acid would enable the maximization of the upconversion luminescence quantum efficiency over a wide range of sizes and growth conditions.

We therefore conducted an eight-reaction screen in WANDA to investigate the dependence of the crystal structure of $NaYF_4$:20% Yb, 2% Er nanoparticles on oleic acid concentration present during synthesis. We rapidly determined the crystal phase composition of the 48 timed aliquots of the eight $NaYF_4$ syntheses by collecting high-throughput XRD (Supporting Information Figure S6) of samples spotted on a 96-well microplate (Figure 1e). Figure 8a displays XRD patterns for $NaYF_4$:20% Yb, 2% Er nanocrystals grown for 1 h with oleic acid−rare earth ion mole ratios (OLA/RE) varying logarithmically from 0 to 2.0. The XRD patterns display peaks that align with the Rietveld-refined peak positions of α- and β-$NaY_{0.78}Yb_{0.20}Er_{0.02}F_4$. At OLA/RE $\leq 10^{-2}$, the mass fraction of β-$NaYF_4$ (f_β) relative to the total mass of $NaYF_4$ remains constant at a baseline level of ~95%, as determined by the Rietveld refinement of the XRD patterns (Figure 8b). Above OLA/RE $= 10^{-2}$, f_β decreases approximately linearly with $\log_{10}$(OLA/RE). By fitting separate lines through the f_β versus log(OLA/RE) data over the two OLA/RE regimes, we can establish a threshold OLA/RE of 0.04, which marks the onset of β-to-α transition. The transition to α-$NaYF_4$ is complete at OLA/RE $= 2.3$, as extracted from the x-intercept of the solid line in Figure 8b. The boundaries of this $\beta \rightarrow \alpha$ transition emphasize the strong correlation between the crystal phase and the upconversion luminescence intensity. The onset and saturation of the $\beta \rightarrow \alpha$ transition coincides with a 10-fold decrease in the upconversion luminescence intensity between 500 and 600 nm (Figure 8b).

The dependence of the crystal structure on the OLA/RE ratio indicates that the binding of oleic acid to α-$NaYF_4$ surfaces stabilizes the α-phase relative to β-$NaYF_4$. Mai et al. have used infrared spectroscopy and transmission electron microscopy to demonstrate that negatively charged oleate ligands bind strongly and electrostatically to the positively charged {100} surfaces of small α-$NaYF_4$ particles.[60] Mai et al.[60] and Yi et al.[61] have both suggested that oleic acid inhibits the propensity of oleylamine to promote

DOI: 10.1021/nl100669s | *Nano Lett.* **2010,** *10,* 1874–1885

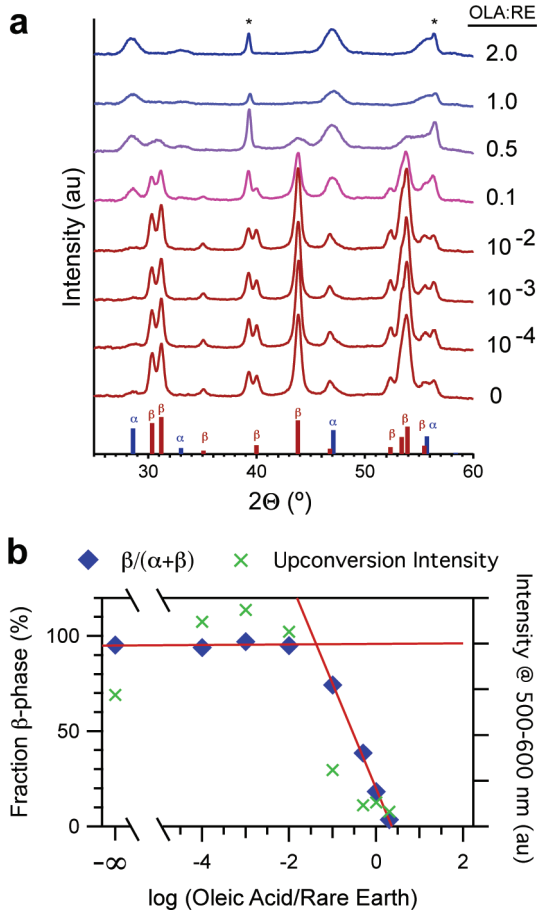

FIGURE 8. (a) $NaYF_4$:20% Yb, 2% Er X-ray diffraction patterns vs oleic acid−rare earth mole ratio. Sticks represent the Rietveld-refined peak positions of α- (blue) and β-$NaY_{0.78}Yb_{0.20}Er_{0.02}F_4$ (red). Asterisks (*) denote cubic NaF byproduct peaks. (b) Mass fraction of β-phase and mass-normalized upconversion luminescence intensity vs log(OLA/RE). The β-phase fraction is determined with Rietveld refinement of the XRD patterns. The dashed (solid) line is the line fit for the first (last) four points on the β-fraction trace. The slope of the solid line is -55 ± 2, the x-intercept is 0.36 (OLA/RE = 2.3), and the intersection of the dashed and solid lines occurs at log(OLA/RE) = -1.38 ± 0.07 (OLA/RE = 0.04).

the formation of β-$NaYF_4$ nanocrystals in predominantly oleylamine solutions.

Yi et al.[61] also demonstrate that in pure oleylamine α-$NaYF_4$ is formed below 320 °C, while β-$NaYF_4$ is formed above 320 °C. Since our reactions are initiated by ramping the temperature of the premixed reaction solution to 330 °C, we must consider the possibility that nanocrystals nucleate initially as α-$NaYF_4$ and later transform into β-$NaYF_4$ at higher temperature. Deliberate two-stage syntheses have been reported previously[60,61] and this phenomenon may explain the residual 5% α-$NaYF_4$ fraction at low OLA/RE. While most of the WANDA reactions showed little structural change over time, aliquot XRD patterns at OLE/RE = 0.5 show that f_β increases gradually over the course of 1 h (Supporting Information Figure S6), consistent with a mechanism in which β-$NaYF_4$ is formed from α-$NaYF_4$ nuclei.

These results demonstrate the structural insight that can be gained through a single, eight-reactor run in WANDA. Staggered sampling of semiparallel reactions and high-throughput XRD of 48 aliquots enable us to monitor the $\beta \rightarrow \alpha$-$NaYF_4$ transition over OLA/RE values and time. While pure oleylamine is the optimal condition for β-$NaYF_4$, the threshold OLA/RE for the onset of the $\beta \rightarrow \alpha$ transition establishes an upper limit when using oleic acid to improve nanocrystal dispersibility and to tune morphology. Most significantly, the case of $NaYF_4$ demonstrates how automated screening of reaction parameters facilitates the high-throughput characterization of structural properties, which can be used maximize the upconversion luminescence that has utility in displays[62] and biological labels.[8]

Conclusion. We have demonstrated a reproducible, robust, and flexible platform for the automated synthesis and characterization of colloidal inorganic nanomaterials. The synthesis of near-identical CdSe samples across eight parallel reactors and over two separate runs demonstrates that even rapid, nucleation-sensitive reactions can be performed reproducibly by precisely defining reaction parameters with automation. The synthesis of CdSe nanocrystals using two separate reaction systems illustrates that WANDA is not constrained to a specific workflow and can utilize reagents that are not compatible with other high-throughput methods. WANDA's flexibility has enabled it to synthesize semiconductor, metal, oxide, and doped nanoparticles with spherical, rod, and nanowire morphologies (Table S1, Figure S7, Supporting Information). WANDA has also synthesized semiconductor heterostructures and ternary semiconductors, highlighting its advantage when performing complex workflows or optimizing reaction systems with large numbers of synthetic variables. With the cases of CdSe, CdTe, and $NaYF_4$:20% Yb,Er nanocrystals, we have demonstrated the ability to screen reaction conditions across multidimensional parameter space to optimize physical properties that have relevance to emerging applications. The optimization of CdSe nanocrystal size and size distribution is crucial to the self-assembly of nanoparticle superlattices, while the optimization of the photoluminescence of CdTe quantum dots enhances the sensitivity of biological labels. Controlling the crystal structure of rare earth-doped $NaYF_4$ has direct implications for the efficiency of upconversion, which is promising for biological and display applications.

The automation of nanomaterials research has broad implications for the fundamental investigation, development, and application of nanomaterials. The ability to iterate rapidly through precisely controlled reaction conditions will facilitate detailed mechanistic studies and enable multivariate analysis that could reveal the principle factors that determine nucleation and growth behavior. WANDA's throughput and flexibility will enable the discovery of new materials through the identification of

DOI: 10.1021/nl100669s | Nano Lett. 2010, 10, 1874–1885

reaction conditions outside conventional synthetic ranges. Our simple empirical model for calculating the diameters of CdSe nanocrystals demonstrates that the results of multidimensional screening can enable accurate predictions for future syntheses. The reproducibility of automation will enable the standardization of recipes, reducing the considerable resources spent attempting to reproduce existing syntheses. The user-friendly and robust nature of WANDA will facilitate the use of nanomaterials in a broad range of applications, since users from disparate fields will be able to obtain the same high quality materials as experienced chemists. We anticipate that the robust, flexible, and accessible nature of this automated synthesis platform will foster the rapid discovery of new materials and facilitate a deeper understanding of the complex and rich chemistry of colloidal nanomaterials.

Acknowledgment. The authors thank M. Caldwell, D. Talapin, T. Mokari, and A. P. Alivisatos for helpful discussions. We thank J. Fisher, R. Fisher, K. Higashihara, R. Rosen, and Symyx Technologies for constructing WANDA. C.X. and A.W.M. were supported by BLUR internships. This work was carried out entirely at the Molecular Foundry and supported by the Office of Science, Office of Basic Energy Sciences, of the U.S. Department of Energy, under capital equipment funds and under Contract No. DE-AC02-05CH11231.

Supporting Information Available. Materials and methods, TEM images of nanomaterials synthesized in WANDA, absorption spectra from manual CdSe syntheses, XRD of CdO byproducts, and time dependent XRD of $NaYF_4$ aliquots. This material is available free of charge via the Internet at http://pubs.acs.org.

REFERENCES AND NOTES

(1) Efros, A. L.; Rosen, M. *Annu. Rev. Mater. Sci.* **2000**, *30*, 475–521.
(2) Murray, C. B.; Norris, D. J.; Bawendi, M. G. *J. Am. Chem. Soc.* **1993**, *115*, 8706–8715.
(3) Shevchenko, E. V.; Talapin, D. V.; Kotov, N. A.; O'Brien, S.; Murray, C. B. *Nature* **2006**, *439*, 55–59.
(4) Sun, S. H.; Murray, C. B. *J. Appl. Phys.* **1999**, *85*, 4325–4330.
(5) Caldwell, M. A.; Raoux, S.; Wang, R. Y.; Wong, H.-S. P.; Milliron, D. J. *J. Mater. Chem.* **2010**, *20*, 1285–1291.
(6) Alivisatos, A. P. *J. Phys. Chem.* **1996**, *100*, 13226–13239.
(7) Bruchez, M.; Moronne, M.; Gin, P.; Weiss, S.; Alivisatos, A. P. *Science* **1998**, *281*, 2013–2016.
(8) Wu, S.; Han, G.; Milliron, D. J.; Aloni, S.; Altoe, V.; Talapin, D. V.; Cohen, B. E.; Schuck, P. J. *Proc. Natl. Acad. Sci. U.S.A.* **2009**, *106*, 10917–10921.
(9) Han, G.; Mokari, T.; Ajo-Franklin, C.; Cohen, B. E. *J. Am. Chem. Soc.* **2008**, *130*, 15811–15813.
(10) Colvin, V. L.; Schlamp, M. C.; Alivisatos, A. P. *Nature* **1994**, *370*, 354–357.
(11) Coe, S.; Woo, W.; Bawendi, M.; Bulovic, V. *Nature* **2002**, *420*, 800–803.
(12) Klein, D. L.; Roth, R.; Lim, A. K. L.; Alivisatos, A. P.; McEuen, P. L. *Nature* **1997**, *389*, 699–701.
(13) Cui, Y.; Banin, U.; Bjork, M. T.; Alivisatos, A. P. *Nano Lett.* **2005**, *5*, 1519–1523.
(14) Talapin, D.; Murray, C. *Science* **2005**, *310*, 86–89.
(15) Urban, J. J.; Talapin, D. V.; Shevchenko, E. V.; Kagan, C. R.; Murray, C. B. *Nat. Mater.* **2007**, *6*, 115–121.
(16) Yin, Y.; Alivisatos, A. P. *Nature* **2005**, *437*, 664–670.
(17) Krishnadasan, S.; Brown, R. J. C.; deMello, A. J.; deMello, J. C. *Lab Chip* **2007**, *7*, 1434–1441.
(18) Murray, C. B.; Kagan, C. R.; Bawendi, M. G. *Annu. Rev. Mater. Sci.* **2000**, *30*, 545–610.
(19) Manna, L.; Scher, E. C.; Alivisatos, A. P. *J. Am. Chem. Soc.* **2000**, *122*, 12700–12706.
(20) Peng, X.; Manna, L.; Yang, W.; Wickham, J.; Scher, E.; Kadavanich, A.; Alivisatos, A. *Nature* **2000**, *404*, 59–61.
(21) Park, J.; Joo, J.; Kwon, S. G.; Jang, Y.; Hyeon, T. *Angew. Chem., Int. Ed.* **2007**, *46*, 4630–4660.
(22) Milliron, D. J.; Hughes, S. M.; Cui, Y.; Manna, L.; Li, J.; Wang, L.-W.; Alivisatos, A. P. *Nature* **2004**, *430*, 190–195.
(23) Liu, H.; Owen, J. S.; Alivisatos, A. P. *J. Am. Chem. Soc.* **2007**, *129*, 305–312.
(24) Chan, E. M.; Alivisatos, A. P.; Mathies, R. A. *J. Am. Chem. Soc.* **2005**, *127*, 13854–13861.
(25) Steckel, J. S.; Yen, B. K. H.; Oertel, D. C.; Bawendi, M. G. *J. Am. Chem. Soc.* **2006**, *128*, 13032–13033.
(26) Joo, J.; Pietryga, J. M.; McGuire, J. A.; Jeon, S.-H.; Williams, D. J.; Wang, H.-L.; Klimov, V. I. *J. Am. Chem. Soc.* **2009**, *131*, 10620–10628.
(27) Wang, F.; Tang, R.; Buhro, W. E. *Nano Lett.* **2008**, *8*, 3521–3524.
(28) Wang, F.; Tang, R.; Kao, J. L.-F.; Dingman, S. D.; Buhro, W. E. *J. Am. Chem. Soc.* **2009**, *131*, 4983–4994.
(29) Carbone, L.; Kudera, S.; Carlino, E.; Parak, W.; Giannini, C.; Cingolani, R.; Manna, L. *J. Am. Chem. Soc.* **2006**, *128*, 748–755.
(30) Maier, W. F.; Stoewe, K.; Sieg, S. *Angew. Chem., Int. Ed.* **2007**, *46*, 6016–6067.
(31) Senkan, S.; Kahn, M.; Duan, S.; Ly, A.; Leidhom, C. *Catal. Today* **2006**, *117*, 291–296.
(32) Kuykendall, T.; Ulrich, P.; Aloni, S.; Yang, P. *Nat. Mater.* **2007**, *6*, 951–956.
(33) Baeck, S.; Jaramillo, T.; Kleiman-Shwarsctein, A.; McFarland, E. *Meas. Sci. Technol.* **2005**, *16*, 54–59.
(34) Whitling, J.; Spreitzer, G.; Wright, D. *Adv. Mater.* **2000**, *12*, 1377–1380.
(35) Belser, K.; Slenters, T. V.; Pfumbidzai, C.; Upert, G.; Mirolo, L.; Fromm, K. M.; Wennemers, H. *Angew. Chem., Int. Ed.* **2009**, *48*, 3661–3664.
(36) Calvin, S.; Carpenter, E.; Cestone, V.; Kurihara, L.; Harris, V.; Brown, E. *Rev. Sci. Instrum.* **2005**, *76*, No. 016103.
(37) Washington, A. L.; Strouse, G. F. *J. Am. Chem. Soc.* **2008**, *130*, 8916–8922.
(38) Nakamura, H.; Yamaguchi, Y.; Miyazaki, M.; Maeda, H.; Uehara, M.; Mulvaney, P. *Chem. Commun.* **2002**, 2844–2845.
(39) Chan, E. M.; Mathies, R. A.; Alivisatos, A. P. *Nano Lett.* **2003**, *3*, 199–201.
(40) Yen, B. K. H.; Stott, N. E.; Jensen, K. F.; Bawendi, M. G. *Adv. Mater.* **2003**, *15*, 1858–1862.
(41) Krishnadasan, S.; Tovilla, J.; Vilar, R.; deMello, A.; deMello, J. *J. Mater. Chem.* **2004**, *14*, 2655–2660.
(42) Yen, B. K. H.; Gunther, A.; Schmidt, M. A.; Jensen, K. F.; Bawendi, M. G. *Angew. Chem., Int. Ed.* **2005**, *44*, 5447–5451.
(43) Shestopalov, I.; Tice, J. D.; Ismagilov, R. F. *Lab Chip* **2004**, *4*, 316–321.
(44) Chan, E. M. Ph.D. Dissertation, University of California at Berkeley, Berkeley, CA, 2006.
(45) Yu, W. W.; Qu, L. H.; Guo, W. Z.; Peng, X. G. *Chem. Mater.* **2003**, *15*, 2854–2860.
(46) Qu, L.; Peng, Z. A.; Peng, X. *Nano Lett.* **2001**, *1*, 333–337.
(47) Zhong, X.; Feng, Y.; Zhang, Y. *J. Phys. Chem. C* **2007**, *111*, 526–531.
(48) Peng, X. G.; Wickham, J.; Alivisatos, A. P. *J. Am. Chem. Soc.* **1998**, *120*, 5343–5344.
(49) Xie, R.; Li, Z.; Peng, X. *J. Am. Chem. Soc.* **2009**, *131*, 15457–15466.
(50) Manna, L.; Milliron, D. J.; Meisel, A.; Scher, E. C.; Alivisatos, A. P. *Nat. Mater.* **2003**, *2*, 382–385.
(51) Owen, J. S.; Park, J.; Trudeau, P.-E.; Alivisatos, A. P. *J. Am. Chem. Soc.* **2008**, *130*, 12279–12281.
(52) Yu, W. W.; Wang, Y. A.; Peng, X. G. *Chem. Mater.* **2003**, *15*, 4300–4308.
(53) Kloper, V.; Osovsky, R.; Kolny-Olesiak, J.; Sashchiuk, A.; Lifshitz, E. *J. Phys. Chem. C* **2007**, *111*, 10336–10341.

DOI: 10.1021/nl100669s | *Nano Lett.* **2010,** *10,* 1874–1885

(54) Bullen, C. R.; Mulvaney, P. *Nano Lett.* **2004**, *4*, 2303–2307.
(55) van Embden, J.; Mulvaney, P. *Langmuir* **2005**, *21*, 10226–10233.
(56) Heer, S.; Kompe, K.; Gudel, H.; Haase, M. *Adv. Mater.* **2004**, *16*, 2102–2105.
(57) Suyver, J.; Grimm, J.; van Veen, M.; Biner, D.; Kramer, K.; Gudel, H. *J. Lumin.* **2006**, *117*, 1–12.
(58) Kramer, K.; Biner, D.; Frei, G.; Gudel, H.; Hehlen, M.; Luthi, S. *Chem. Mater.* **2004**, *16*, 1244–1251.
(59) Mai, H.-X.; Zhang, Y.-W.; Si, R.; Yan, Z.-G.; Sun, L.-D.; You, L.-P.; Yan, C.-H. *J. Am. Chem. Soc.* **2006**, *128*, 6426–6436.
(60) Mai, H.-X.; Zhang, Y.-W.; Sun, L.-D.; Yan, C.-H. *J. Phys. Chem. C* **2007**, *111*, 13730–13739.
(61) Yi, G. S.; Chow, G. M. *Adv. Funct. Mater.* **2006**, *16*, 2324–2329.
(62) Downing, E.; Hesselink, L.; Ralston, J.; Macfarlane, R. *Science* **1996**, *273*, 1185–1189.

DOI: 10.1021/nl100669s | *Nano Lett.* **2010,** *10,* 1874–-1885